IEEE Access
Multidisciplinary | Rapid Review | Open Access Journal

Received April 7, 2019, accepted April 18, 2019, date of publication April 23, 2019, date of current version May 20, 2019.

Digital Object Identifier 10.1109/ACCESS.2019.2912804

Risk Assessment of Distribution Networks Integrating Large-Scale Distributed Photovoltaics

LEI WANG[1], MINYU YUAN[1], FAN ZHANG[1], XULI WANG[2], LEI DAI[2], AND FENG ZHAO[3]

[1]Anhui Provincial Laboratory of Renewable Energy and Energy Saving, Hefei University of Technology, Hefei 230009, China
[2]Economical Technical Institute, State Grid Anhui Electric Power Co. Ltd., Hefei 230071, China
[3]State Grid Anhui Electric Power Co., Ltd., Hefei 230071, China

Corresponding author: Minyu Yuan (yuanminyu11@163.com)

This work was supported in part by the National Key R&D Program of China under Grant 2016YFB0900601, and in part by the Anhui Provincial Laboratory of Renewable Energy and Energy Saving under Grant 45000-411104/012.

ABSTRACT Risk impacts on the operation of electric power distribution networks, when large amounts of distributed photovoltaics (PVs) are included, are gradually increasing to become a critical consideration for distribution networks' operations. In this paper, a risk assessment method is proposed which considers large-scale distributed PV feeding into distribution networks. Cluster partitioning is used to group large-scale distributed PV, to more accurately calculate the operational risk indicators for distribution networks with large-scale distributed PV compared to traditional risk assessment methods. A copula function is used to describe the correlation between the PV output and the load, in order to more accurately calculate power flow information compared to the traditional independent model of output and load. Node voltages over-limits and branch power flows outside boundaries are selected as the risk indicators, and a comprehensive risk indicator is introduced to more comprehensively and meaningfully evaluate the risk of distribution networks' operation. Also, the effects on the operational risk of the distribution network of load fluctuations, and, PV quantity, capacity, and location are analyzed and discussed. Finally, the IEEE34-bus system was simulated, and the results for different scenarios were calculated and analyzed. The simulation results demonstrate the effectiveness of the proposed method.

INDEX TERMS Distributed, large-scale, photovoltaics, risk assessment.

I. INTRODUCTION

Solar energy is rapidly developing, and photovoltaic (PV) power generation for input to electric power grids is one of its main applications. Compared with traditional power generation technology, PV power generation has outstanding advantages in terms of abundant sunlight resources, cleanliness, freedom from noise and pollution. It has received more and more attention and development [1], [2]. The time-domain output power from PV generation is random and uncertain [3]. When PV power sources are connected to distribution networks, large-scale [4], the many distributed small-capacity PV sources drive changes in the entire distribution network flows. These flows are different from traditional distribution network power flows. It can bring new problems in power quality, power flow distribution, system loss, security and stability of distribution networks [5]–[8]. It is of great importance to evaluate the reliability and safety of distribution networks' operation with large amounts of distributed PV power generation.

In recent years, methods for systematic risk assessment of distribution networks with distributed generation have been gradually established. Risk assessment models support the foundations of power system design [9]. The main components of distribution networks include distribution lines, transformers, user loads, circuit breakers and so on [10]. Therefore, risk assessment of distribution networks with distributed generation mainly studies distributed power models, component outage model for various types of power distribution equipment and load models [11]. In terms of PV power generation, the solar radiation intensity obeys a Beta distribution over short periods. Then, according to the linear relationship between PV output and solar radiation, the Beta distribution model for the PV output power is

The associate editor coordinating the review of this manuscript and approving it for publication was Giambattista Gruosso.

derived [12], [13]. The probabilistic model for PV power output is based on the theory of non-parametric kernel density estimation, as was proposed in [14] which improved the modeling of PV's output statistical distribution. The random fluctuations loads also create risks for the safe and stable operation of distribution networks [15]. A normal distribution approximation is usually used to characterize the uncertainty of continuous loads. Samper [16] conducted a risk assessment for planning for the high penetration of solar PV installations in distribution systems. Modified risk-adjusted cost ratios are used to optimize the size and allocation of battery energy storage systems (BESS), considering distributed PV generation, uncertainties in weather conditions, PV penetration, load growth, and the costs of BESS.

As a very important aspect of distribution network assessment, risk assessment deepens and further develops deterministic and probabilistic assessment methods [17], [18], combining the probability of accidents with their consequences, and quantitatively reflects the risks to the distribution networks' operation [19]. There are now many methods for risk assessment of distribution networks, which can be categorized as analytical methods, simulation methods, and mixed methods combining analytical and simulation–based approaches [20], [21]. The analytical method established a reliability probability model according to the structure of the system and the logical relationship within it. The model is solved accurately by means of recursion or iteration. The probability of each possible fault and the loss of distribution networks' function after the fault occurs are calculated by means of fault enumeration. Thus, system-level risk indicators are comprehensively formed [22]. When the analytical method is used, the probability distribution of the state of distribution networks can be calculated by using a Gram-Charlier series expansion and the dynamic probability power flow algorithm which is based on semi-invariant additivity [23]. Current simulation methods are generally based on Monte Carlo simulation [24], [25], which can extract random numbers subject to an arbitrary distribution. According to the individual probability distributions of loads, distribution network components, and weather conditions [26], a random sampling is used to select the parameters, form a system state sequence, and then analyze the generated state set. When this simulation approach is used, the probability distribution of the state of the distribution networks is calculated by Monte Carlo sampling of the probability distribution of PV output power [27].

The ultimate purpose of risk assessment is to obtain the statistics indicating the quantitative risk level of system, to guide planning and operation of the distribution networks [28], [29]. In order to reasonably reflect the risk level of a system, current risk assessment indicators generally focus on two aspects: the probabilities of abnormal state occurrences, and, the consequences of those possible abnormal states. Zhang *et al.* [30] considers the impact of capacity and location on a single PV access point and uses the risk index on the node voltage limit and branch flow limit to assess the risk of distribution network. Li *et al.* [31] established a probability and severity model of line overload for when there was wind power connected to the grid. Considering the temporal uncertainty of wind power, and the probability and consequences of line load fluctuations, a Cholesky decomposition was used to model the correlation between load and power. A point estimation method was used to calculate the risk indicator for active line power overloads [9]. In addition, the optimal power flow model [32], [33] can be used to calculate the risk indicators of system load shedding, voltage over-limit [34], [35], and so on.

For the power system, the output characteristics of PV power generation are quite different from traditional dispatchable power generation. The above literature provides a good research basis for the risk assessment of distribution networks that integrate PVs. However, for risk assessment of distribution networks integrating large-scale distributed PVs, more technical requirements and improved methods are needed. The contributions of this work are: (i) clustering distributed PVs before conducting risk assessment on distribution network that integrate large-scale distributed PVs; (ii) probabilistic power flow models that take into account distributed PV and load correlations for risk assessment; (iii) Propose a comprehensive risk indicator for voltage and power flow limits, considering the impact of load fluctuations and the number, capacity, and locations of large-scale distributed PVs on risk.

Bearing these ideas in mind, the remainder of this paper is arranged as follows. Section II explains the cluster partition of large-scale distributed PVs. Section III explains the stochastic model of the distribution network components; Section IV explains the risk indicators for over-limits node voltages and off-limits branch power flows, and comprehensive risk indicator. Section V shows the simulation results and analysis of distribution network integrating large-scale distributed PVs. Finally, Section VI offers the conclusions from this research.

II. LARGE-SCALE DISTRIBUTED PHOTOVOLTAICS CLUSTER PARTITON

"Large-scale distributed PVs" has not been clearly defined so far. According to the current status of equipment and operation of distribution networks in China, the "large-scale distributed PVs" means that the number of effective nodes that the PVs directly connect to can reach 30% or more of the number of nodes in distribution networks. The effective node means that the PV capacities of this node reaches at least 20% of the transformer capacities within this node. The number of PVs is high in distribution networks with large-scale distributed PVs, and it would be very complicated to simulate each PV in detail. Therefore, this paper considers the clustering method to group PVs with similar characteristics into clusters for more practical simulation.

A. CLUSTER INDICATOR

Some of the PVs in power systems with large-scale distributed PVs have similar characteristics. Clusters can be grouped according to indicators as follows.

1) ACTIVE POWER REGULATION CAPACITY P_r

When the voltage level of a system is too high and its reactive power regulation capability is limited, the active power of distributed PVs can be reduced to ensure that the system operates at a safe voltage level. The range of active power output regulation is:

$$P_r \in [0, P_{MPPT}] \tag{1}$$

$$P_{MPPT} = \sum_{j=1}^{n} P_{jMPPT} \tag{2}$$

where P_{MPPT} is the active power of distributed PVs under its maximum power point tracking control mode, and P_{jMPPT} is the active output of PVs under maximum power point tracking control mode of the j-th PV inverters within the node.

2) REACTIVE POWER REGULATION CAPACITY Q_r

Reactive power regulation capacity is one of the important criteria for cluster partitions. When emergency situations such as regional faults occur, the cluster can provide necessary reactive power support for the region. When the system voltage level is too high, the reactive output of PVs can be adjusted to ensure that the system operates at a good voltage level. The reactive power regulation range of distributed PVs is:

$$Q_r \in [Q_{\min}, Q_{\max}] \tag{3}$$

$$\begin{cases} Q_{\min} = \sum_{j=1}^{n} Q_{j\min} \\ Q_{\max} = \sum_{j=1}^{n} Q_{j\max} \end{cases} \tag{4}$$

$$\begin{cases} Q_{j\min} = -\sqrt{S_j^2 - P_{jMPPT}^2} \\ Q_{j\max} = \sqrt{S_j^2 - P_{jMPPT}^2} \end{cases} \tag{5}$$

where $Q_{\min}$ and $Q_{\max}$ are the capacitive and inductive reactive power of the node respectively, $Q_{j\min}$ and $Q_{j\max}$ are the capacitive and inductive reactive power of the j-th PV inverters within the node, respectively, and S_j is the rated capacity of the PV inverters.

B. DYNAMIC CLUSTER

The cluster partition of large-scale distributed PVs is similar to community structure. The characteristics of nodes within the cluster are similar, and the characteristics of clusters are quite different. Therefore, the community theory can be used to achieve a reasonable partition for cluster with large-scale distributed PVs. First, the partition indicators are normalized and the weights are determined, then the similarity matrix of the distributed PVs is calculated, and finally the cluster is created using the modularity function.

1) NORMALIZATION OF PARTITION INDICATORS

In order to eliminate the dimensional influence among the various indicators proposed in the previous section, each indicator should be normalized. The normalization formula is shown in (6):

$$x'_{im} = \frac{x_{im} - \min(x_{im})}{\max(x_{im}) - \min(x_{im})} \tag{6}$$

where $x_{im}$is the m-th partition indicator of the i-th node, $\max(x_{im})$ and $\min(x_{im})$ are the maximum and minimum values of the m-th indicator of the i-th node, respectively, and $x'_{im}$is the m-th indicator of the i-th node after normalization.

2) CONSTRUCTING the SIMILARITY MATRIX

The similarity between two nodes is calculated using a scalar method. A similarity matrix is then formed. The more similar the two nodes are, the closer the elements in the similarity matrix are to 1. The formula is shown in (7)-(8):

$$r(i,j) = \begin{cases} 1, & i = j \\ \left[\frac{1}{L}\sum_{m=1}^{2} \alpha_k \left(x_{ij} \cdot x_{jm}\right)\right], & i \neq j \end{cases} \tag{7}$$

$$\mathrm{L} = \max\left(\sum_{m=1}^{2} \alpha_k \left(x_{ij} \cdot x_{jm}\right)\right), \quad i \neq j \tag{8}$$

where α_k is the weight of the m-th indicator, and x_{jm} is the m-th indicator of the j-th node.

3) THE MODULARITY FUNCTION AND THE PARTITION ALGORITHM

Considering a single distributed PV source as a node, each node has a connecting edge and the weight of the connecting edge is the similarity of the distributed PV sources. The distributed PV network is constructed. The modularity function [36] is an indicator for community structure: the closer the modularity function value Q is to 1, the more reasonable the community partition results are. Cluster and community structures have similar characteristics. Their calculation is shown by (9):

$$Q = \frac{1}{2s}\sum_{i,j}\left(g_{ij} - \frac{s_i s_j}{2s}\right)\delta\left(G_i, G_j\right) \tag{9}$$

where g_{ij} is the edge of the network, s_i and s_j are the sum of the weights of edges on the nodes i and j, respectively, s is the weight of all edges in network. VariableG_i is the cluster where node i is located: when $G_i = G_j$, δ =1, otherwise δ =0.

The Fast Unfolding [37] cluster algorithm is used to partition clusters. First, each node acts as a cluster separately and then nodes are merged according to the gradient for increase of the Q-value function, to obtain a new cluster until the value of Q no longer increases. Finally, the optimal partition for the distributed PV cluster is obtained.

III. STOCHASTIC MODEL OF SYSTEM COMPONENTS

Since PV systems' outputs and loads have strong uncertainties, they are modeled from a probabilistic perspective.

A. STOCHASTIC OUTPUT PROBABILITY MODEL FOR LARGE-SCALE DECENTRALIZED PHOTOVOLTAICS

In this paper, the non-parametric kernel density estimation method is used to describe the stochastic model for PV generation at each node. Suppose $P_1, P_2, \ldots, P_n$ are n samples of PV output power P, and the probability density function of the output power is $f_{pv}(p)$. Then, the kernel estimate of $f_{pv}(p)$ is:

$$\hat{f}_{PV}(p) = \frac{1}{nh}\sum_{i=1}^{n} K\left(\frac{p-P_i}{h}\right) \tag{10}$$

where K is the kernel function of kernel density estimation, h is the bandwidth, and n is the sample capacity.

According to the theory of kernel density estimation, when $n \to \infty$, $h \to 0$ and $nh \to \infty$, $\hat{f}_{PV}(p)$ will converge to $f_{pv}(p)$, so the accuracy of the kernel density estimation depends on the bandwidth and the kernel function. When bandwidth h is constant, the performance of kernel density estimation of different kernel functions is almost the same [14], so the choice of bandwidth has a great deal of influence on fitting the kernel density estimation. If the value of h is too large, it will cause $\hat{f}_{PV}(p)$ to be excessively smooth, mask some structural features of $f_{pv}(p)$, and a large estimation bias occurs; if the value of h is too small, the deviation will decrease, which will make $\hat{f}_{PV}(p)$ less smooth and $f_{pv}(p)$ will have larger fluctuations.

ISE (Integrated Square Error) can be used to measure whether a kernel density estimation function $\hat{f}_{PV}(p)$ is a good estimate of the probability density function $f_{pv}(p)$:

$$ISE\left(\hat{f}_{PV}\right) = \int \left(\hat{f}_{PV}(p) - f_{PV}(p)\right)^2 dp \tag{11}$$

Next, the expected value of ISE to get the MISE (Mean Integrated Square Error) is found:

$$\begin{aligned}
&MISE\left(\hat{f}_{PV}\right) \\
&= E\left(\int \left(\hat{f}_{PV}(p) - f_{PV}(p)\right)^2 dp\right) \\
&= \int E^2\left(\hat{f}_{PV}(p) - f_{PV}(p)\right) dp \\
&\quad + \int D\left(\hat{f}_{PV}(p) - f_{PV}(p)\right) dp \\
&= \int Bias^2\left(\hat{f}_{PV}(p)\right) dp + \int Var\left(\hat{f}_{PV}(p)\right) dp \\
&= \int \left(\left(\frac{h^2}{2}\right)\mu(K) f''(p) + o\left(h^2\right)\right)^2 dp \\
&\quad + \int \left(\left(\frac{1}{nh}\right) R(K) f(p) + o\left(\frac{1}{nh}\right)\right) dp \\
&= \frac{h^4}{4}\mu^2(K) R\left(f''\right) + \frac{1}{nh} R(K) + o\left(\frac{1}{nh}\right) + o\left(h^4\right)
\end{aligned} \tag{12}$$

$$\mu(K) = \int x^2 K(x) dx \tag{13}$$

$$R(K) = \int K^2(x) dx \tag{14}$$

$$R\left(f''\right) = \int \left(f''_{PV}(p)\right)^2 dp \tag{15}$$

where $Bias\left(\hat{f}_{PV}(p)\right)$ and $Var\left(\hat{f}_{PV}(p)\right)$ are the deviations and variances of kernel density estimation, respectively.

Omitting the high-order term in (12) to obtain the AMISE (Asymptotic Mean Integrated Square Error) leads to:

$$AMISE\left(\hat{f}_{PV}\right) = \frac{h^4}{4}\mu^2(K) R\left(f''\right) + \frac{1}{nh} R(K) \tag{16}$$

Taking the partial derivative of (16) and using the optimal bandwidth where AMISE reaches its minimum value gives:

$$h_{AMISE} = \left(\frac{R(K)}{\mu^2(K) R\left(f''\right)}\right)^{1/5} n^{-1/5} \tag{17}$$

The final kernel density estimate of $f_{pv}(p)$ can be obtained by bringing the optimal bandwidth into (10).

B. LOAD PROBABILITY MODEL

Loads estimates are obtained from forecasts, so there are uncertainties. This paper uses a normal distribution approximation to characterize the uncertainty of loads. Assuming that the expected value and the variance of a load's active and reactive power are μ_P, σ_P^2, and μ_Q, σ_Q^2, respectively, the probability density functions for active and reactive power are, respectively:

$$f(P) = \frac{1}{\sqrt{2\pi}\sigma_P} \exp\left(-\frac{(P-\mu_P)^2}{2\sigma_P^2}\right) \tag{18}$$

$$f(Q) = \frac{1}{\sqrt{2\pi}\sigma_Q} \exp\left(-\frac{(Q-\mu_Q)^2}{2\sigma_Q^2}\right) \tag{19}$$

IV. SYSTEM RISK INDICATOR

This paper mainly considers the risk of output disturbances of large-scale distributed PVs and the load fluctuation to the good operation of a distribution network. Without considering the system failure, the indicators for evaluation of node over-voltages and off-limits branch power flows are established to quantitatively evaluate the safety risk level of a system. Using the probability distribution of node voltages and probabilistic branch load flows, the probability density function and the cumulative distribution function can be obtained. According to the cumulative distribution function, the probability of exceeding the voltage limits at each node and the power flow through each network branch can be obtained. The risk level can be determined by the severity indicator.

A. RISK INDICATOR FOR OVER-LIMIT NODE VOLTAGES

It is necessary to establish a voltage risk indicator. Lower voltages increase the power and energy loss in a distribution network. Lower voltage also affects the stability of distribution network operation and can lead to system collapses and large area power outages. When the voltages are too high, it effects the insulation of power equipment.

The probability formulas of voltages exceeding the upper and lower limits of node voltage are as follows:

$$\begin{cases} P_r\left(\bar{V}_i\right) = P_r\left(V_i > V_{i\max}\right) = 1 - F\left(V_{i\max}\right) \\ P_r\left(\underline{V}_i\right) = P_r\left(V_i < V_{i\min}\right) = F\left(V_{i\min}\right) \end{cases} \tag{20}$$

The voltage offset is used as a severity consequence function in the risk definition. The upper and lower limits of node voltages are calculated as follows:

$$Sev\left(\underline{V}_i\right) = \begin{cases} \dfrac{V_{i\min} - V_i}{V_{\min}}, & V_i < V_{i\min} \\ 0, & V_i \geq V_{i\min} \end{cases} \tag{21}$$

$$Sev\left(\overline{V}_i\right) = \begin{cases} \dfrac{V_{i\max} - V_i}{V_{\max}}, & V_i > V_{i\max} \\ 0, & V_i \leq V_{i\max} \end{cases} \tag{22}$$

where V_i represents the voltage amplitude of at node i,V_{imax} and V_{imin} are the upper and lower limits of the voltage amplitudes allowed by node i, respectively, and $F(V)$ represents the cumulative node voltage distribution function.

The risk indicator of node voltage over-limit is then:

$$Rv = \max\left(P_r\left(\overline{V}_i\right) Sev\left(\overline{V}_i\right), P_r\left(\underline{V}_i\right) Sev\left(\underline{V}_i\right)\right) \tag{23}$$

B. RISK INDICATOR FOR OFF-LIMITS BRANCH POWER FLOW

When the power flow in a line is within its normal range, it has little influence on outage probability of that line; when the power flow in a line is greater than its thermal stability limit, the line overload and overcurrent protection devices operate. The larger the power flow, the smaller the protection action time, and the smaller the possibility of adopting control measures to reduce the power flow to within the normal range and the greater the probability that the line will trip. Disconnecting the line could lead to loss of power supply for users and result in serious economic losses. Therefore, for the risk assessment of distribution systems integrating large-scale distributed PVs, we must pay attention to the problem of branch overload and set up risk indicators for it.

In calculating a line's over-limit probability, only the upper limit of the branch is considered, and the probability of the branch flow exceeding its limits is calculated as:

$$P_r(S_{ij}) = P_r(S_{ij} > S_{ijmax}) = 1 - F(S_{ijmax}) \tag{24}$$

The severity function for branch overload is as follows:

$$Sev\left(S_{ij}\right) = \left|\frac{S_{ij} - S_{ij\max}}{S_{ij\max}}\right| \tag{25}$$

where S_{ij} is the active power of branch ij, and S_{ijmax} is the upper limit of active power allowed by branch ij. Assuming that the upper limit is 1.3 times the normal value, and that the normal value is the expected value of branch power when distributed power is not connected; $F(S_{ij})$ represents the cumulative distribution function for branch power flow.

The risk indicator for branch power flow rising above its limit is:

$$Rs = P_r(S_{ij})Sev(S_{ij}) \tag{26}$$

C. COMPREHENSIVE INDICATOR

In this paper, the entropy weighted method [38] is used to calculate the weight of indicators for over-limit node voltages and over-limit branch power flows. Then, the comprehensive indicator of risk assessment is calculated. Supposing that there are m nodes with n risk assessment indicators (n=2, indicators of voltage over-limit and branch power flow off-limit), the original quantity matrix is:

$$R = (r_{\mathrm{ij}})_{\mathrm{m\times n}} \tag{27}$$

where $i = m, j = n = 2$, and r_{ij} is the evaluation value of the j-th indicator of the i-th node.

The steps for calculating the weight of each indicator are:

Step1: Calculate the proportion P_{ij} of the j-th index value in the i-th node:

$$p_{ij} = r_{ij} \Big/ \sum_{i=1}^{m} r_{ij} \tag{28}$$

Step2: Calculate the entropy value e_j of the j-th indicator in all nodes:

$$e_j = -k \sum_{i=1}^{m} \left(p_{ij} \cdot \ln p_{ij}\right) ik = 1/\ln mj \tag{29}$$

Step3: Calculate the entropy weightW_j of the j-th indicator:

$$W_j = \left(1 - e_j\right) \Big/ \sum_{j=1}^{n} \left(1 - e_j\right) \tag{30}$$

The comprehensive risk assessment indicator is:

$$R = R_v W_1 + R_s W_2 \tag{31}$$

where W_1 and W_2 are the weights for indicators of node voltages rising over their limits and over-limit branch power flows, respectively, and R_v and R_s are the risk indicators of node voltage over-limit and branch power flow outside boundaries, respectively.

The flowchart for the risk assessment considering large-scale distributed PVs feeding into a distribution network is shown in Fig. 1.

V. SIMULATION RESULTS AND DISCUSSION

According to the evaluation model and indicators, a cluster is selected to calculate the risk based on the IEEE34-bus distribution network system and using the MATLAB platform. According to the voltage level of different scales of distributed PV sources, as shown in Table 1, the total capacity of distributed PV sources of the medium voltage distribution network (10 kV) should be between 0.4 MW and 6 MW. The reference voltage of the system is 24.9 kV. The reference voltage of the root node is 1.03 p.u., or 25.64 kV. The reference capacity of the system is 1 MVA.

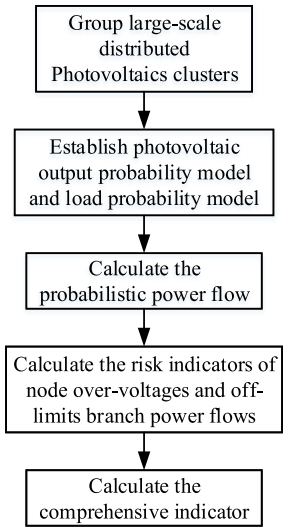

FIGURE 1. Flowchart of risk assessment, considering large-scale distributed photovoltaics feeding into a distribution network.

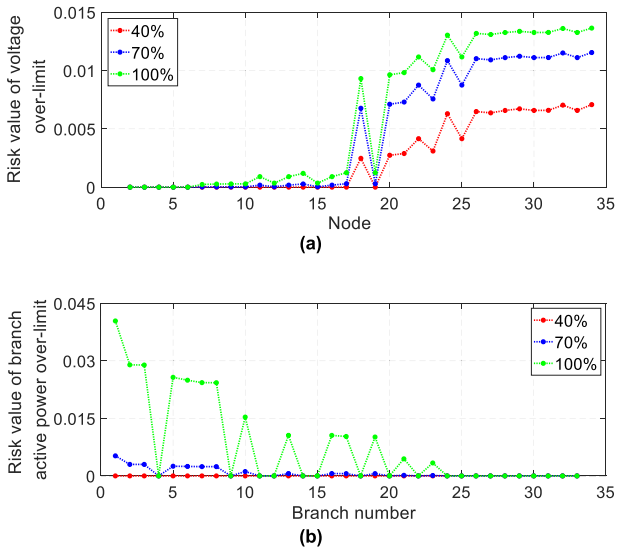

FIGURE 2. Risk indicators for different load fluctuations. (a) Risk indicator for each over-limit node voltage. (b) Risk indicator for each off-limit branch active power.

TABLE 1. Voltage levels for different scales of distributed pv.

Photovoltaic capacity	Connection voltage level
8 kW	220 V
8~400 kW	380 V
400~6000 kW	10 kV
5000~30000 kW	35 kV

A. IMPACT OF LOAD FLUCTUATIONS ON SYSTEM RISK

The impact of load fluctuations on the system risk were studied without any distributed PV in the distribution system. It was assumed that the nodes' loads follow the normal distribution. Their expected values were the original load of the system. The standard deviation was assumed to be 40%, 70%, and 100% of the expected value. In this example, node 1 was considered to be the equilibrium node, and all other nodes were considered to be PQ nodes. Risk indicators for each over-limit node voltage and off-limit branch power flow could be obtained. Comparisons of results for different standard deviations are shown in Fig. 2.

When the standard deviations of load stochastic model increases, it means that the fluctuations of load are larger, which means there is a risk of exceeding the limit of node voltage and branch current. From Fig. 2(a), it can be seen that under the same standard deviation, the risk values of each over-limit node voltage increases with the increase of the node number. Nodes 19, 23, 25, and 33 belong to the edge node of the distribution network system, and risk values falls sharply with this trend. For different standard deviations values, the number of over-limit nodes increases with the increasing standard deviation. Also, the risk value of over-limit voltages at each node is also larger, and risk values for over-limit voltages at each node for a standard deviation of 100% were doubled when compared with that of 40%.

From Fig. 2(b), it can be seen that for the same standard deviation, the risk of off-limit active power at each branch decreases with the increase of the branch number. Branch numbers of 4, 9, 11, 12, 14, 15, 18, 20, 22, and 24 are lateral branches of the distribution network system, thus showing a sharp drop. For different standard deviations, as the standard deviation increases, the number of over-limit branches increase, and risk of over-limit active power at each branch also increases. When the standard deviation is 100%, the risk of the active power exceeding the power limit of each branch is four times higher than it is for a standard deviation of 70%. In practice, the risk caused by load fluctuations to a system can be reduced from the perspective of suppressing the load fluctuations.

B. IMPACT OF THE QUANTITY OF LARGE-SCALE DISTRIBUTED PHOTOVOLTAICS SOURCES ON SYSTEM RISK

The joint probability density of PV output and load with a capacity of 200 kW is shown in Fig. 3. From Fig. 3 it can be seen that the joint probability density model of the PV

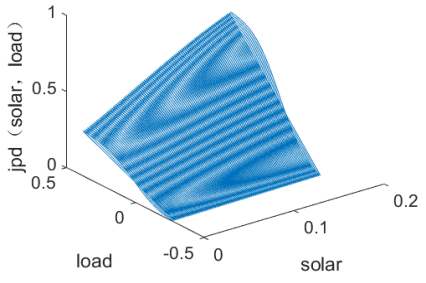

FIGURE 3. Joint probability density of photovoltaics output and load.

output and the load, based on copula theory, better reflects the correlation between them. The copula function [39] is a function that connects the joint distributions of multidimensional random variables with their one-dimensional marginal distributions and describes the correlations between variables. The joint probability distributions of the PV sources and the load is obtained by using the copula function. The probabilistic power flow was calculated using the semi-invariant method. The probability density functions and cumulative distribution functions of each random variable were obtained using the Gram-Charlier series expansion.

For the following examples, it was assumed the expected load value at a node is the original system load value, and the standard deviations were 20% of the expected value. Comparative analysis was carried out for three cases with no distributed PV sources, 10 nodes (randomly select nodes 2, 4, 15, 20, 22, 23, 31, 32, 33 and 34) with distributed PVs, and 20 nodes (randomly add nodes 6, 7, 8, 12, 14, 16, 18, 19, 21 and 25 based on 10 nodes) with distributed PVs. Taking node 10 and branch 27 as examples, the probability density curves of the node voltages and branch active power quantities are shown in Fig. 4.

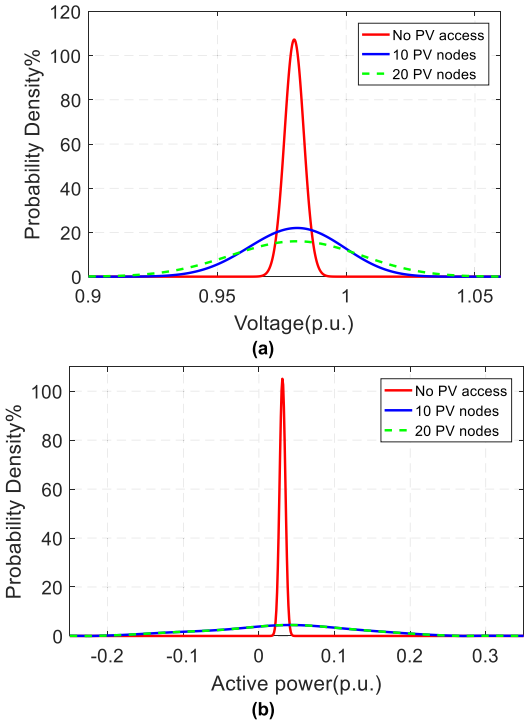

FIGURE 4. Probability density curve for different PV source quantities. (a) Probability density curve for node voltages. (b) Probability density curves for branch active power.

From Fig. 4, it can be seen that when there is no distributed PVs, the selected node voltage fluctuates in the range of 0.966-0.994 p.u., and the active power value of selected branch is in the range of 0.017-0.046 p.u. When there are 10 nodes including distributed PVs, the voltage fluctuations are in the range of 0.923-1.034 p.u. and active power value is in the range of -0.208-0.256 p.u. When there are 20 nodes including distributed PVs, the voltage fluctuations are in the range of 0.901-1.055 p.u. and active power values are in the range of -0.210-0.258 p.u. The number of PV sources has an impact on the node voltages and branch power flows of the distribution network system. The inclusion of PV sources increases the voltage fluctuations' ranges, and those fluctuation ranges increase as the number of PV sources increases. Also, multiple nodes containing PVs can the active power of a selected branch have a negative value, which signifies changes in the original system's power flow distribution, and even changes in the direction of branches' power flow.

The risk indicators for over-limit node voltage and over-limit branch active power under different PV source quantities are shown in Fig. 5.

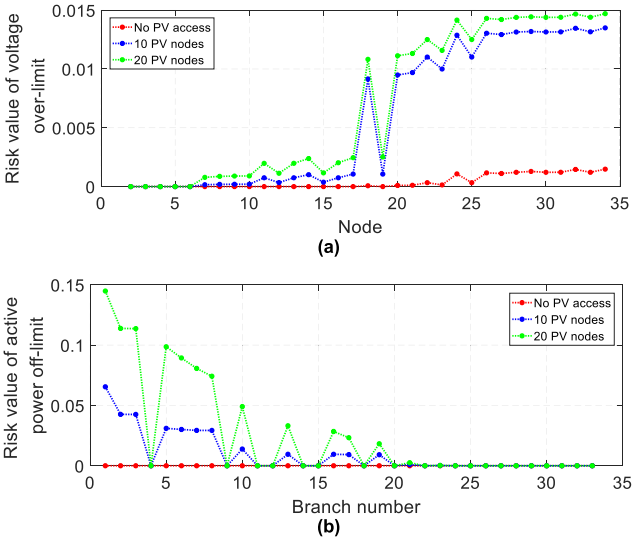

FIGURE 5. Risk indicators for different PV source quantities. (a) Indicators for each node voltage over-limit risk. (b) Indicator of each branch's over-limit active power.

From Fig. 5, it can be seen that increasing the numbers of PV sources will lead to increasing risk indicators for node over-limit voltage and over-limit branch active power. The risk of over-limit branch active power with twenty nodes containing PVs is 1.2 times higher than it is with ten nodes containing PVs.

C. IMPACT OF THE CAPACITY OF LARGE-SCALE DISTRIBUTED PHOTOVOLTAIC SOURCES ON SYSTEM RISK

The following example assumes that the expected load value of a node is the nominal load system value, and the standard deviation is 20% of expected value. With PV sources connected to 20 nodes of the system, comparative analysis was carried out for three cases where the capacity of each node was 100 kW, 200 kW and 300 kW. Taking node 10 and branch 27 as examples, the probability densities of node voltages and branch active power flows were obtained as shown in Fig. 6.

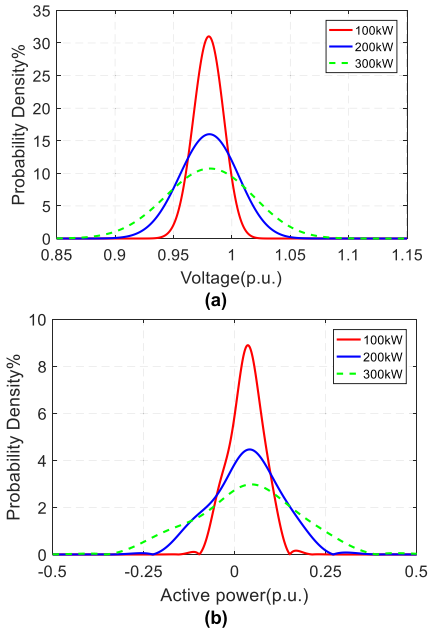

FIGURE 6. Probability density curves for different PV source capacities. (a) Probability density curve for node voltage. (b) Probability density curve of branch active power.

From Fig. 6(a), it can be seen that when PV sources with a capacity of 100 kW are connected to twenty nodes, the selected node voltage fluctuates within the range of 0.937-1.021 p.u. When the PV source capacity was 200 kW, the selected node voltages fluctuated within the range of 0.901-1.055 p.u. When the PV source capacity was 300 kW, the selected node voltages fluctuated in the range of 0.867-1.088 p.u. It can be seen that voltage fluctuation ranges increase with increase PV capacity. From Fig. 6(b), it can be seen that when PV sources with a capacity of 100 kW are respectively connected to ten nodes, the active power value of the selected branch is between -0.093 and 0.148 p.u. When the PV capacity source was 200 kW, the active power value was between -0.208 and 0.256 p.u. When the PV source capacity was 300 kW, the active power value was between -0.319 and 0.361 p.u. The change of PV capacity changes the original power flow distribution, and the range of the active power value increases with increasing PV source capacity.

The risk indicators for node voltage that go over limits and branch active power outside limits with different PV source capacities are shown in Fig. 7.

From Fig. 7(a), it can be seen that when PV sources with a capacity of 100 kW are connected to ten nodes, the maximum risk value of voltages going over-limits at all nodes is 0.108. When the capacity is 200 kW, the maximum risk value is 0.147. When the capacity is 300 kW, the maximum risk value is 0.172. When PV sources with a capacity of 300 kW are connected, the risk value of the voltage over-limit is 0.6 times higher than it is with PV sources with a capacity of 100 kW. From Fig. 7(b), it can be seen that risk value of active power off-limit increases with the increase of PV source capacity. When PVs with a capacity of 300 kW is connected, the risk of over-limit active power is 20 times higher than that of 200 kW.

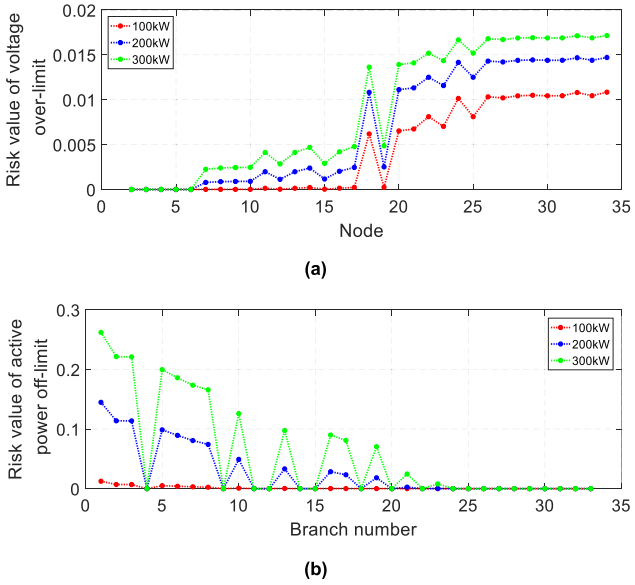

FIGURE 7. Risk indicators for different photovoltaics source capacities. (a) Risk indicator for each node voltage going over-limit. (b) Risk indicator for each branch active power going outside its limit.

D. IMPACT OF THE SOURCE LOCATIONS OF LARGE-SCALE DISTRIBUTED PHOTOVOLTAICS ON SYSTEM RISK

With 150kW PVs connected to ten nodes (node 2, 4, 15, 20, 22, 23, 31, 32, 33 and 34), the input node was changed from node 22 to node 11. Risk indicators for over-limit voltage and active power values in this case are shown in Fig. 8.

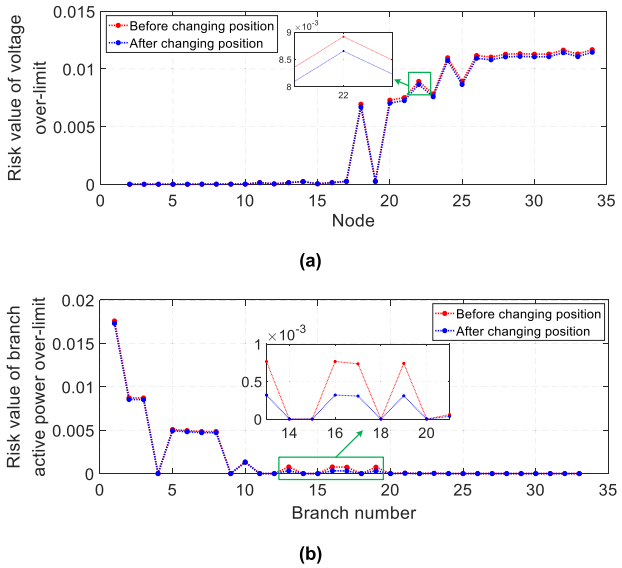

FIGURE 8. Risk indicators when changing PV source locations. (a) Risk indicator for each node voltage going over-limit. (b) Risk indicators for each branch's active power going over its limit.

TABLE 2. comprehensive risk indicator.

Node	Risk indicator for over-limit node voltages	Risk indicator for over-limit branch power flows	Comprehensive risk indicator
2	0.0000	0.0176	0.0118
3	0.0000	0.0087	0.0059
4	0.0000	0.0087	0.0058
5	0.0000	0.0000	0.0000
6	0.0000	0.0051	0.0034
7	0.0000	0.0050	0.0033
8	0.0000	0.0048	0.0033
9	0.0000	0.0048	0.0033
10	0.0000	0.0000	0.0000
11	0.0001	0.0014	0.0010
12	0.0000	0.0000	0.0000
13	0.0001	0.0000	0.0000
14	0.0002	0.0008	0.0006
15	0.0000	0.0000	0.0000
16	0.0001	0.0000	0.0000
17	0.0003	0.0008	0.0006
18	0.0069	0.0007	0.0028
19	0.0003	0.0000	0.0001
20	0.0073	0.0007	0.0029
21	0.0075	0.0000	0.0025
22	0.0089	0.0001	0.0030
23	0.0078	0.0000	0.0026
24	0.0110	0.0066	0.0036
25	0.0089	0.0000	0.0029
26	0.0112	0.0000	0.0037
27	0.0110	0.0000	0.0036
28	0.0113	0.0000	0.0037
29	0.0113	0.0000	0.0037
30	0.0113	0.0000	0.0037
31	0.0113	0.0000	0.0037
32	0.0116	0.0000	0.0038
33	0.0113	0.0000	0.0037
34	0.0117	0.0000	0.0038

From Fig. 8(a), it can be seen that when change PVs from node 22 to node 11, the value of the risk of node the voltage going over-limit around node 22 is decreased by 3%. It can be seen from the above comparison, the influence of PVs on the voltage of the distribution network depends mainly on the electrical distance between one node and the node containing PVs. If the electrical distance to a PV source is very short, the risk of that node voltage going over its limits will be relatively large. From Fig. 8(b), it can be seen that after moving the PV source, the risk of active power going outside its limits, between nodes 11 and 22 (branch 11-14, 14-17, 17-18 and 18-20) is reduced by 58%. This is related to the electrical distance between the PV access point and the branch, and also to the load carried by the branch.

E. COMPREHENSIVE INDICATOR

In this section, risk indicators for node voltages going outside their limits, and branch active power over-limits in the previous section are selected, that is, when 150 kW of PV sources

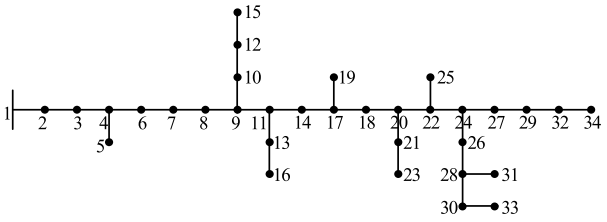

FIGURE 9. The structure of the IEEE34-bus distribution network system.

TABLE 3. The load parameters of the ieee34-bus distribution network system.

Node	Active load（p.u.）	Reactive load（p.u.）
2	1.91×10^{-2}	9.87×10^{-3}
4	5.29×10^{-3}	2.74×10^{-3}
9	1.30×10^{-4}	7.00×10^{-5}
10	1.13×10^{-2}	5.84×10^{-3}
11	1.49×10^{-2}	7.71×10^{-3}
12	1.18×10^{-2}	2.34×10^{-2}
13	2.06×10^{-3}	1.07×10^{-3}
17	1.24×10^{-3}	6.40×10^{-4}
20	4.37×10^{-3}	2.26×10^{-3}
22	1.00×10^{-2}	5.17×10^{-3}
23	2.70×10^{-2}	2.16×10^{-2}
24	5.00×10^{-2}	5.00×10^{-2}
26	4.66×10^{-2}	2.97×10^{-2}
27	3.04×10^{-3}	1.57×10^{-3}
28	1.31×10^{-2}	6.77×10^{-3}
29	1.49×10^{-1}	1.49×10^{-2}
30	9.20×10^{-3}	4.76×10^{-3}
31	8.86×10^{-3}	7.09×10^{-3}
32	7.54×10^{-3}	3.90×10^{-3}
34	1.95×10^{-2}	1.34×10^{-1}

are connected to nodes 2, 4, 15, 20, 22, 23, 31, 32, 33 and 34. Comprehensive indicators can quickly reflect the overall risk of a location. It is calculated by the entropy weight method. The comprehensive risk indicators for each node excluding balanced nodes are shown in Table 2.

VI. CONCLUSION

This paper proposes a risk assessment method considering power distribution networks that integrate large-scale distributed PVs. High distributed PVs are clustered for faster simulation while maintaining accuracy. Risk indicators for node voltage going outside limits and branch active power flows over limits are calculated for the selected clusters. Then, a comprehensive risk indicator is obtained, and the risks to the distribution network's performance are comprehensively evaluated. Simulations verify the effects of load fluctuations, PV quantities, PV capacities, and different PV locations on the operational risks to the distribution network, and proving the effectiveness of the proposed method. In practice, we can reduce risk of to the performance distribution networks by reducing the fluctuations of load and

TABLE 4. The branch parameters of the ieee34-bus distribution network system.

Branch number	Start node	End node	Resistance（p.u.）	Reactance（p.u.）	Density/2（p.u.）
1	1	2	2.03×10^{-3}	8.95×10^{-4}	4.50×10^{-7}
2	2	3	1.36×10^{-3}	6.00×10^{-4}	3.00×10^{-7}
3	3	4	2.54×10^{-2}	1.12×10^{-2}	5.50×10^{-6}
4	4	5	4.60×10^{-3}	2.03×10^{-3}	1.00×10^{-6}
5	4	6	2.95×10^{-2}	1.30×10^{-2}	6.50×10^{-6}
6	6	7	2.34×10^{-2}	1.03×10^{-2}	5.00×10^{-6}
7	7	8	7.87×10^{-4}	3.47×10^{-4}	0.00
8	8	9	2.44×10^{-4}	1.08×10^{-4}	0.00
9	9	10	1.34×10^{-3}	5.93×10^{-4}	2.50×10^{-7}
10	9	11	8.04×10^{-3}	3.54×10^{-3}	1.50×10^{-6}
11	10	12	3.79×10^{-2}	1.67×10^{-2}	8.00×10^{-6}
12	11	13	6.61×10^{-4}	2.91×10^{-4}	1.00×10^{-7}
13	11	14	2.39×10^{-3}	1.05×10^{-3}	5.00×10^{-8}
14	12	15	1.08×10^{-2}	4.76×10^{-3}	2.35×10^{-5}
15	13	16	1.61×10^{-2}	7.09×10^{-3}	3.55×10^{-5}
16	14	17	4.09×10^{-4}	1.80×10^{-4}	0.00
17	17	18	2.90×10^{-2}	1.28×10^{-2}	6.00×10^{-6}
18	17	19	1.84×10^{-2}	8.10×10^{-3}	4.05×10^{-5}
19	18	20	7.87×10^{-4}	3.47×10^{-4}	0.00
20	20	21	3.06×10^{-3}	6.58×10^{-3}	3.00×10^{-6}
21	20	22	3.86×10^{-3}	1.70×10^{-3}	5.00×10^{-7}
22	21	23	8.31×10^{-3}	3.66×10^{-3}	1.50×10^{-6}
23	22	24	4.59×10^{-3}	2.02×10^{-3}	1.00×10^{-6}
24	22	25	1.28×10^{-3}	5.62×10^{-4}	2.50×10^{-7}
25	24	26	1.59×10^{-3}	7.01×10^{-4}	5.00×10^{-8}
26	24	27	2.20×10^{-4}	9.71×10^{-5}	5.00×10^{-9}
27	26	28	2.10×10^{-3}	9.30×10^{-4}	5.00×10^{-7}
28	27	29	1.06×10^{-3}	4.68×10^{-4}	2.00×10^{-7}
29	28	30	2.20×10^{-4}	9.72×10^{-5}	5.00×10^{-9}
30	28	31	6.77×10^{-4}	2.98×10^{-4}	1.50×10^{-7}
31	29	32	2.87×10^{-3}	1.26×10^{-3}	5.00×10^{-7}
32	30	33	2.56×10^{-3}	1.68×10^{-3}	5.00×10^{-7}
33	32	34	4.17×10^{-4}	1.84×10^{-4}	5.00×10^{-8}

controlling the number, capacity and location of access points for PV sources.

APPENDIX

The structure of the IEEE34-bus distribution network system is shown in Figure 9. Load and branch parameters of the IEEE34-bus distribution network system are presented in Table 3 and Table 4.

REFERENCES

[1] F. Dinçer, "The analysis on photovoltaic electricity generation status, potential and policies of the leading countries in solar energy," *Renew. Sustain. Energy Rev.*, vol. 15, no. 1, pp. 713–720, Jan. 2011.

[2] F. Liu, R. Li, Y. Li, R. Yan, and T. Saha, "Takagi–Sugeno fuzzy model-based approach considering multiple weather factors for the photovoltaic power short-term forecasting," *IET Renew. Power Gener.*, vol. 11, no. 10, pp. 1281–1287, Aug. 2017.

[3] M. Yang and X. Huang, "Ultra-short-term prediction of photovoltaic power based on periodic extraction of PV energy and LSH algorithm," *IEEE Access*, vol. 6, pp. 51200–51205, Sep. 2018.

[4] M. Ding, Z. Xu, W. Wang, X. Wang, Y. Song, and D. Chen, "A review on China's large-scale PV integration: Progress, challenges and recommendations," *Renew. Sustain. Energy Rev.*, vol. 53, pp. 639–652, Jan. 2016.

[5] S. H. Madaeni, R. Sioshansi, and P. Denholm, "Comparing capacity value estimation techniques for photovoltaic solar power," *IEEE Trans. Photovolt.*, vol. 3, no. 1, pp. 407–415, Jan. 2013.

[6] K. Kamono and Y. Ueda, "Real-time estimation of areal photovoltaic power using weather and power flow data," *IEEE Trans. Sustain. Energy*, vol. 9, no. 2, pp. 754–762, Apr. 2018.

[7] R. A. Walling, R. Saint, R. C. Dugan, J. Burke, and L. A. Kojovic, "Summary of distributed resources impact on power delivery systems," *IEEE Trans. Power Del.*, vol. 23, no. 3, pp. 1636–1644, Jul. 2008.

[8] Y. Ju, W. Wu, B. Zhang, and H. Sun, "An extension of FBS three-phase power flow for handling pv nodes in active distribution networks," *IEEE Trans. Smart Grid*, vol. 5, no. 4, pp. 1547–1555, Jul. 2014.

[9] M. Negnevitsky, D. H. Nguyen, and M. Piekutowski, "Risk assessment for power system operation planning with high wind power penetration," *IEEE Trans. Power Syst.*, vol. 30, no. 3, pp. 1359–1368, May 2015.

[10] M. E. Baran and F. F. Wu, "Network reconfiguration in distribution systems for loss reduction and load balancing," *IEEE Trans. Power Del.*, vol. 4, no. 2, pp. 1401–1407, Apr. 1989.

[11] Q. Chen, T. Littler, S. Han, and W. Haifeng, "Risk assessment model for wind generator tripping off," in *Proc. CSEE*, Feb. 2015, vol. 35, no. 3, pp. 576–582.

[12] I. Abouzahr and R. Ramakumar, "Loss of power supply probability of stand-alone photovoltaic systems: A closed form solution approach," *IEEE Trans. Energy Convers.*, vol. 6, no. 1, pp. 1–11, Mar. 1991.

[13] S. Karaki, R. B. Chedid, and R. Ramadan, "Probabilistic performance assessment of autonomous solar-wind energy conversion systems," *IEEE Trans. Energy Convers.*, vol. 14, no. 3, pp. 766–772, Sep. 1999.
[14] W. Yan, Z. Ren, X. Zhao, J. Yu, Y. Li, and X. Hu, "Probabilistic photovoltaic power modeling based on nonparametric kernel density estimation," *Autom. Electr. Power Syst.*, vol. 37, no. 10, pp. 35–40, May 2013.
[15] S. Dai, D. Niu, and Y. Li, "Daily peak load forecasting based on complete ensemble empirical mode decomposition with adaptive noise and support vector machine optimized by modified grey wolf optimization algorithm," *Energies*, vol. 11, no. 1, pp. 163–187, Jan. 2018.
[16] M. E. Samper, F. A. Eldali, and S. Suryanarayanan, "Risk assessment in planning high penetrations of solar photovoltaic installations in distribution systems," *Int. J. Elect. Power Energy Syst.*, vol. 104, pp. 724–733, Jan. 2019.
[17] E. Ciapessoni, D. Cirio, S. Grillo, S. Massucco, A. Pitto, and F. Silvestro, "An integrated platform for power system security assessment implementing probabilistic and deterministic methodologies," *IEEE Syst. J.*, vol. 7, no. 4, pp. 845–853, Dec. 2013.
[18] Y. Feng, W. Wu, B. Zhang, and W. Li, "Power system operation risk assessment using credibility theory," *IEEE Trans. Power Syst.*, vol. 23, no. 3, pp. 1309–1318, Aug. 2008.
[19] Z. H. Quan, L. I. Jingshu, and L. I. Ruijin, "Fast assessment of power failure risk in distribution network containing distributed generation," *Power System Technol.*, vol. 38, no. 4, pp. 882–887, Apr. 2014.
[20] D. K. Khatod, V. Pant, and J. Sharma, "Analytical approach for well-being assessment of small autonomous power systems with solar and wind energy sources," *IEEE Trans. Energy Convers.*, vol. 25, no. 2, pp. 535–545, Jun. 2010.
[21] P. Zhang, Y. Wang, W. Xiao, and W. Li, "Reliability evaluation of grid-connected photovoltaic power system," *IEEE Trans. Sustain. Energy*, vol. 3, no. 3, pp. 379–389, Jul. 2012.
[22] Z. Bie and X. Wang, "The application of Monte Carlo method to reliability evaluation of power systems," *Autom. Electr. Power Syst.*, vol. 21, no. 6, pp. 68–75, Jun. 1997.
[23] W. Zhu, X. Chen, K. Yu, and W. Wei, "Operation risk analysis of smart distribution network based on dynamic probability power flow," in *Proc. IEEE PES Innov. Smart Grid Technol.*, Tianjin, China, May 2012, pp. 1–6.
[24] W. EI-Khattam, Y. G. Hegazy, and M. M. A. Salama, "Investigating distributed generation systems performance using Monte Carlo simulation," *IEEE Trans. Power Syst.*, vol. 21, no. 2, pp. 524–530, May 2006.
[25] A. B. Rodrigues and M. G. Da Silva, "Probabilistic assessment of available transfer capability based on Monte Carlo method with sequential simulation," *IEEE Trans. Power Syst.*, vol. 22, no. 1, pp. 484–492, Feb. 2007.
[26] X. Li and H. Wang, "Operation risk assessment of wind farm integrated system influenced by weather conditions," in *Proc. IEEE Power Energy Soc. Gen. Meeting*, Vancouver, BC, Canada, Jul. 2013, pp. 1–5.
[27] S. V. Dhople and A. D. Dominguez-Garcia, "Estimation of photovoltaic system reliability and performance metrics," *IEEE Trans. Power Syst.*, vol. 27, no. 1, pp. 554–563, Feb. 2012.
[28] M. Ni, J. D. McCalley, V. Vittal, and T. Tayyib, "Online risk-based security assessment," *IEEE Trans. Power Syst.*, vol. 18, no. 1, pp. 258–265, Feb. 2003.
[29] M. Ni *et al.*, "Software implementation of online risk-based security assessment," *IEEE Trans. Power Syst.*, vol. 18, no. 3, pp. 1165–1172, Aug. 2003.
[30] H. Zhang *et al.*, "Research on risk assessment in distribution network with PV generations," in *Proc. IEEE 3rd Int. Conf. Integr. Circuits Microsyst. (ICICM)*, Shanghai, China, Nov. 2018, pp. 249–253.
[31] X. Li, X. Zhang, L. Wu, P. Lu, and S. Zhang, "Transmission line overload risk assessment for power systems with wind and load-power generation correlation," *IEEE Trans. Smart Grid*, vol. 6, no. 3, pp. 1233–1242, May 2015.
[32] X. Bai, L. Qu, and W. Qiao, "Robust AC optimal power flow for power networks with wind power generation," *IEEE Trans. Power Syst.*, vol. 31, no. 5, pp. 4163–4164, Sep. 2016.
[33] S. S. Guggilam, E. Dall'Anese, Y. C. Chen, S. V. Dhople, and G. B. Giannakis, "Scalable optimization methods for distribution networks with high PV integration," *IEEE Trans. Smart Grid*, vol. 7, no. 4, pp. 2061–2070, Jul. 2016.
[34] H. Wan, J. D. McCalley, and V. Vittal, "Risk based voltage security assessment," *IEEE Trans. Power Syst.*, vol. 15, no. 4, pp. 1247–1254, Nov. 2000.
[35] A. B. Almeida, E. V. De Lorenci, R. C. Leme, A. C. Z. De Souza, B. I. L. Lopes, and K. Lo, "Probabilistic voltage stability assessment considering renewable sources with the help of the PV and QV curves," *IET Renew. Power Gener.*, vol. 7, no. 5, pp. 521–530, Sep. 2013.
[36] X. Dou, L. Chang, C. Ni, X. Duan, P. Ge, and Z. Wu, "Multi-level dispatching and control of active distribution network for virtual cluster of distribution photovoltaic," *Autom. Electr. Power Syst.*, vol. 42, no. 3, pp. 21–31, Feb. 2018.
[37] V. D. Blondel, J.-L. Guillaume, and R. Lambiotte, E. Lefebvre, "Fast unfolding of communities in large networks," *J. Stat. Mech.-Theory Exp.*, no. 10, 2008, Art. no. P10008. doi: 10.1088/1742-5468/2008/10/P10008.
[38] J. Lu, W. Wang, Y. Zhang, and S. Cheng, "Multi-objective optimal design of stand-alone hybrid energy system using entropy weight method based on HOMER," *Energies*, vol. 10, no. 10, pp. 1664–1680, Oct. 2017.
[39] L. Zhou, D. Zhang, C. Li, H. Li, and W. Huo, "Access capacity analysis considering correlation of distributed photovoltaic power and load," *Autom. Electr. Power Syst.*, vol. 41, no. 4, pp. 56–61, Feb. 2017.

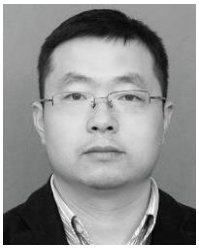

LEI WANG was born in 1978. He received the B.E. and M.E. degrees in electrical engineering from the Hefei University of Technology, Hefei, Anhui, China, in 2000 and 2003, respectively, and the Ph.D. degree from the Hefei institutes of Physical Science, CAS, Hefei, Anhui, China, in 2010.

He is currently an Associate Professor with the School of Electrical Engineering and Automation, Hefei University of Technology. His research interests include renewable energy and its application, and simulation and control of power transmission.

Dr. Wang was a recipient of the Anhui Provincial Science and Technology Progress Award, in 2017.

MINYU YUAN was born in 1994. She received the B.E. degree in electrical engineering from the Hefei University of Technology, Hefei, Anhui, China, in 2013, where she is currently pursuing the M.E. degree.

Since 2017, she has been a postgraduate with the Anhui Provincial Laboratory of New Energy Utilization and Energy Conservation, Hefei University of Technology, Hefei. Her research interests include risk assessment and the simulation of renewable energy in power systems.

FAN ZHANG was born in 1994. He received the B.E. degree in electrical engineering from the Hefei University, Hefei, Anhui, China, in 2012.

Since 2017, he has been a postgraduate with the Anhui Provincial Laboratory of New Energy Utilization and Energy Conservation, Hefei University of Technology, Hefei. His research interests include risk assessment and the simulation of renewable energy in power systems.

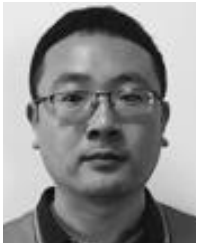

XULI WANG was born in 1984. He received the B.E. degree in electrical engineering from Shandong University, Jinan, Shandong, China, in 2007.

He is currently a Senior Engineer with the Economic and Technological Research Institute, State Grid Anhui Electric Power Co., Ltd. His research interests include distribution network planning, renewable energy and its application.

LEI DAI was born in 1982. He received the B.E. degree in electrical engineering from the Shanghai University of Electric Power. Shanghai, China, in 2004.

He is currently an Electrical Engineer with the Economic and Technological Research Institute of State Grid Anhui Electric Power Co., Ltd. His research interests include grid planning and new energy consumption.

FENG ZHAO was born in 1985. He received the B.E. degree in electrical engineering from Tsinghua University, in 2008.

He is currently a Senior Researcher with State Grid Anhui Electric Power Co., Ltd. His research interests include distribution power grid planning, renewable energy management, and electric power system reform.